Magn Reson Med Sci 2019; 18; 150–157
doi:10.2463/mrms.mp.2018-0004
Published Online: November 9, 2018

MAJOR PAPER

Diffusion Tensor Imaging of the Brachial Plexus: A Comparison between Readout-segmented and Conventional Single-shot Echo-planar Imaging

Michael J. Ho[1,2*], Alexander Ciritsis[1], Andrei Manoliu[3], Bram Stieltjes[4], Magda Marcon[1], Gustav Andreisek[5], and Felix Pierre Kuhn[1]

Purpose: Diffusion tensor imaging (DTI) adds functional information to morphological magnetic resonance neurography (MRN) in the assessment of the brachial nerve plexus. To determine the most appropriate pulse sequence in scan times suited for diagnostic imaging in clinical routine, we compared image quality between simultaneous multi-slice readout-segmented (rs-DTI) and conventional single-shot (ss-DTI) echo-planar imaging techniques.

Methods: Institutional Review Board (IRB) approved study including 10 healthy volunteers. The supraclavicular brachial plexus, covering the nerve roots and trunks from C5 to C7, was imaged on both sides with rs-DTI and ss-DTI. Both sequences were acquired in scan times <7 min with *b*-values of 900 s/mm^2 and with isotropic spatial resolution.

Results: In rs-DTI image, the overall quality was significantly better and distortion artifacts were significantly lower ($P = 0.001–0.002$ and $P = 0.001–0.002$, respectively) for both readers. In ss-DTI, a trend toward lower degree of ghosting and motion artifacts was elicited (reader 1, $P = 0.121$; reader 2, $P = 0.264$). No significant differences between the two DTI techniques were found for signal-to-noise ratios (SNR), contrast-to-noise ratios (CNR) and fractional anisotropy (FA) ($P \geq 0.475$, $P \geq 0.624$, and $P \geq 0.169$, respectively). Interreader agreement for all examined parameters and all sequences ranged from intraclass correlation coefficient (ICC) 0.064 to 0.905 and Kappa 0.40 to 0.851.

Conclusion: Incomparable acquisition times rs-DTI showed higher image quality and less distortion artifacts than ss-DTI. The trend toward a higher degree of ghosting and motion artifacts in rs-DTI did not deteriorate image quality to a significant degree. Thus, rs-DTI should be considered for functional MRN of the brachial plexus.

Keywords: *brachial plexus, diffusion tensor imaging peripheral nerves, diffusion-weighted imaging, medical representative, neurography*

Introduction

MRI has recently emerged as the preferred imaging technique for the evaluation of the brachial plexus by virtue of its capability to provide an excellent soft tissue contrast in the delineation of nerves and trunks course.[1,2] Optimized T_2-weighted sequences with homogenous fat suppression, referred to as magnetic resonance neurography (MRN) have proofed to be valuable in depicting brachial plexopathies, such as nerve compression, tumor, trauma, or inflammatory diseases.[3–7] The major challenge in using MRN for the recognition of brachial plexus disease resides in the fact that the identification of nerve damages is mainly based on the evaluation of nerve morphologic features and signal alterations leading to inherent specificity and sensitivity limitations.[8–10] Recent studies have suggested that diffusion tensor imaging (DTI) of the brachial plexus, by depicting intrinsic features of nerve tissues microstructure on a molecular level, usefully contribute to the differential diagnosis of brachial plexopathies[11–14] beyond conventional morphologic MRN.

[1]Institute of Diagnostic and Interventional Radiology, University Hospital Zurich, 100 Rämistrasse, Zurich 8091, Switzerland
[2]Department of Neuroradiology, University Hospital Freiburg, Freiburg, Germany
[3]Department of Psychiatry, Psychotherapy and Psychosomatics, Psychiatric Hospital, University of Zurich, Zurich, Switzerland
[4]Department of Radiology, University of Basel, Basel, Switzerland
[5]Department of Radiology, Cantonal Hospital Münsterlingen, Münsterlingen, Switzerland
*Corresponding author, Phone: +41-44-255-29-00, Fax: +41-44-255-44-43, E-mail: michael.ho@usz.ch

Received: January 15, 2018 | Accepted: July 11, 2018

In clinical practice, strong susceptibility-related artifacts like geometric distortions and signal loss caused by spin dephasing, apart from long acquisition times, restrict the implementation of DTI in standard imaging protocols for the evaluation of the brachial plexus. In the currently widely used conventional single-shot echo-planar DTI (ss-DTI), small isotropic voxels are combined with a large FOV to achieve the complete coverage of the emerging nerve roots, bilaterally, from C5 to T_1, while limiting the signal loss of the nerve tissue and decreasing partial volume effects. An alternative, recently introduced technique, which divides the *k*-space trajectory into multiple segments in the readout direction, limits susceptibility artifacts and geometric distortion.[15–17] This so-called readout-segmented echo-planar DTI (rs-DTI) sequence uses multiple excitations followed by short echo-trains for the sampling of the tissue diffusion data, part by part, to then combine it to a final image.[15] Due to briefer echo-trains and shorter echo-spacing, in comparison to conventional ss-DTI sequences, rs-DTI is capable of achieving a higher image resolution, an increased signal-to-noise-ratio (SNR) and a reduction of susceptibility-based artifacts. New rs-DTI has been applied previously in pelvic imaging,[18] prostate imaging,[19] cerebral imaging,[20,21] and lumbar nerve root imaging.[22] A direct comparison of ss-DTI and rs-DTI techniques for DTI of the brachial plexus is desirable before implementation in clinical routine and has not been performed yet. Therefore, the aim of this study was to compare standard axial single-shot echoplanar imaging with an advanced read-out segmented technique with respect to image quality and measurement of relevant quantitative DTI parameters while keeping the total acquisition time comparable for both sequences and acceptable for a routine clinical setting.

Methods

Written informed consent from all 10 healthy volunteers was received after the local ethics board had approved this prospective study. Five women, age (mean ± standard deviation [SD]) 29.2 ± 3.6 years, age range 26–35 years; 5 men, age (mean ± SD) 32.8 ± 6.0 years, age range 24–40 years were examined between May and December 2015. Exclusion criteria were: age younger than 18 years; history of systemic disorders; acute or chronic neck pain; any known plexopathy or systemic neuropathy; prior brachial plexus or cervical spine surgery; and contraindication to MRI.

Image acquisition

Morphological and diffusion tensor images of the supraclavicular brachial plexus of both sides were acquired on a 3T MR system (MAGNETOM Skyra, Siemens Healthcare, Erlangen, Germany) with a commercially available 64-channel head-neck coil and an 18-channel body coil.

Two DTI data sets were acquired: first, as a standard of reference, ss-DTI images in the axial plane with scan parameters according to current literature and second rs-DTI images in the axial plane with a prototype simultaneous multi-slice RESOLVE technique. Isotropic voxels with diameters of 2.4 mm were acquired with both DTI sequences allowing for multi-planar reformatting. *B*-values were set to 0 and 900 s/mm^2 for both sequences and acquisition time was 6 min 30 sec and 6 min 45 sec for ss-DTI and rs-DTI, respectively.

An isotropic T_2-weighted sampling perfection with the application of optimized contrasts using different flip angle evolution (SPACE) sequence with short tau inversion recovery (STIR) fat saturation was performed in the coronal plane for better anatomical orientation. Additional pulse sequences specific parameters are outlined in Table 1.

Image analysis

All obtained data was anonymized (subject's initials blinded) and stored in the local picture archiving and communication (PACS) system (IMPAX 6.0, Agfa HealthCare, Mortsel, Belgium). Images were post-processed with the medical imaging interaction toolkit (MITK) diffusion toolkit (German Cancer Research Center, Heidelberg, Germany, www.mitk.org). Two readers independently carried out quantitative and qualitative images assessment (reader 1, AM: clinical fellow in musculoskeletal radiology with a PhD in neuroimaging; reader 2, MH: research fellow in musculoskeletal radiology with 2 years training in neuroradiology).

SNR measurements

For the SNR quantification, both readers independently placed an ellipsoid ROI for each subject into an area of homogeneous signal within the intervertebral disc between the fifth and sixth cervical vertebra, in both DTI series. The mean signal intensity

Table 1 Sequence of parameters

	ss-DTI	rs-DTI	SPACE STIR
b-value 1/2 (s/mm^2)	0/900	0/900	–
Averages *b*-value 1/2	2/5	2/2	–
Simultaneously excited slices	1	2	–
TR (ms)	5800	3030	3500
TE (ms)	59	57	166
FOV (mm^2)	250 x 250	250 x 250	205 x 205
In plane resolution (mm^2)	2.4 x 2.4	2.4 x 2.4	0.8 x 0.8
Number of slices	42	42	144
Stacks	1	1	1
Slice thickness (mm)	2.4	2.4	0.8
Pixel bandwidth (Hz/px)	2004	1265	454
Acquisition time (min:s)	06:30	06:45	07:11

rs-DTI, readout-segmented echo planar diffusion-tensor imaging; SPACE STIR, sampling perfection with application of optimized contrasts using different flip angle evolution short tau inversion recovery; ss-DTI, single-shot echo planar diffusion-tensor imaging.

and the corresponding SD were extracted. Subsequently, SNR was defined as the ratio of the obtained mean signal intensity of the ROI-based measurement and its SD.[22]

CNR measurements

The contrast ratio (C) between the trunks of the brachial plexus and the surrounding musculature was evaluated by measuring their corresponding signal intensity (I) using the following formula: $C = \frac{I(\text{nerve}) - I(\text{muscle})}{I(\text{nerve}) + I(\text{muscle})}$. In order to perform I measurements, circular ROIs were placed into the trunks of both sides of the supraclavicular plexus just distally to the root ganglion C7 and in the adjacent medial scalene muscle, in both DTI series. The ROI size was meticulously adjusted to the size of the trunk to minimize partial volume effects. For CNR, calculation C was divided by the estimated noise standard deviation (see SNR).

Fractional anisotropy measurement

Nerve structure integrity was assessed by measuring and subsequently interpreting fractional anisotropy (FA) values. For this purpose, in the TRACE image obtained from the post-processing of the DTI data, a ROI with a diameter adjusted to the cross-sectional area of the nerve structure was placed at level of the trunks from C5 to T_1, distally to the nerve root ganglion for both sides. The ROI was then registered to the corresponding FA map to extract the FA value (Fig. 1).

Qualitative image evaluation

Both diffusion sequences, ss-DTI and rs-DTI, were graded by applying a semi-quantitative 5-point Likert scale evaluating the presence of potential geometrical distortions, ghosting/motion artifacts and resolution (1, none; 2, low; 3, moderate; 4, high; 5, very high) and to rate overall image quality (1, excellent; 2, good; 3, moderate; 4, poor; 5, non-diagnostic) both diffusion sequences were compared to the corresponding SPACE STIR image as the reference standard (Figs. 2 and 3).

Statistical analysis

For the performance of all statistical testing, IBM SPSS statistics, version 21 (IBM Corporation, Armonk, NY, USA) was used.

Quantitative image analysis

Descriptive statistics was used to report mean values of CNR and SNR measurements across the study population, performed by the two readers, for both ss-DTI and rs-DTI.

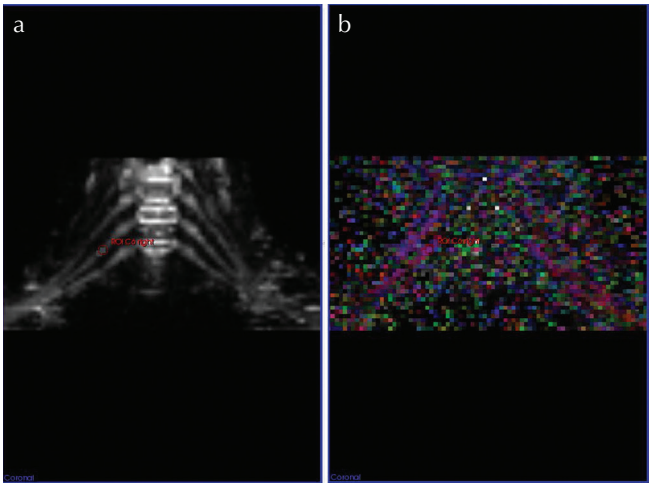

Fig. 1 ROI-based fractional anisotropy (FA) measurement in a 33-year old male volunteer. For the assessment of nerve structure integrity FA values were measured with MITK diffusion toolkit (German Cancer Research Center, Heidelberg, Germany; www.mitk.org). In the trace image (**a**) an ROI, in diameter adjusted to the cross-sectional area of the nerve structure, was placed in the trunk just distally of the nerve root ganglion. The ROI was then registered to the corresponding FA map (**b**) in order to extract the FA value.

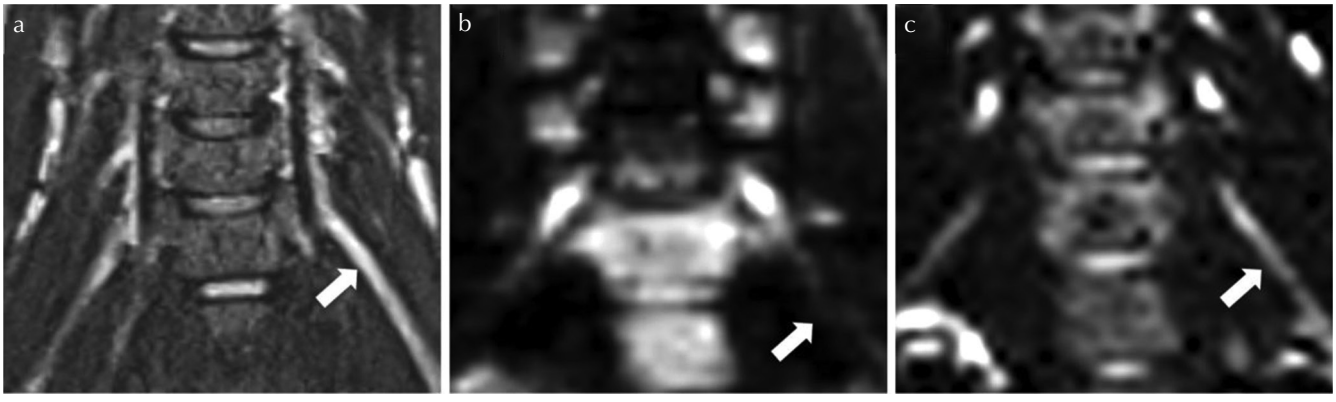

Fig. 2 Distortion artifacts observed with single-shot echo planar diffusion-tensor imaging (ss-DTI) for a 36-year old male healthy volunteer. (**a**) shows the SPACE STIR image with delineation of the root C7 left (arrow) as standard of reference for anatomical correlation; (**b**), the corresponding ss-DTI image with a distortion artifact in the course of the root C7 left (arrow); in (**c**) the rs-DTI image depicts the root C7 left without major distortion. In this case, geometrical distortion artifacts for ss-DTI were graded "high"[4] by both readers, whereas geometrical distortions artifacts for readout-segmented echo planar diffusion-tensor imaging (rs-DTI) were rated "low" by reader 1 and "moderate" by reader 2.

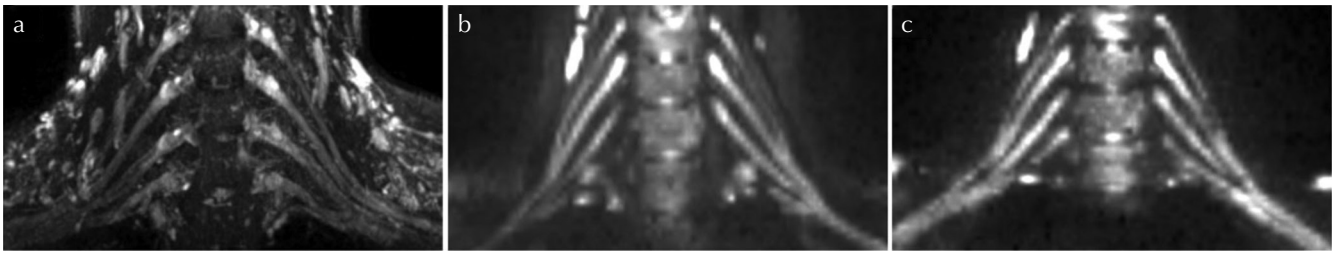

Fig. 3 The image quality of diffusion tensor imaging of brachial plexus for a 26-year old female healthy volunteer. For anatomical correlation of diffusion tensor images (**a**) shows a maximum intensity projection (slab thickness 14.0 mm) of a sampling perfection with the application of optimized contrasts using different flip angle evolution, short tau inversion recovery (SPACE STIR) image covering all nerve roots and trunks from C5 to C7. Corresponding maximum intensity projections (slab thickness 14.0 mm) for an single-shot echo planar diffusion-tensor imaging (ss-DTI) tensor image in panel (**b**) and for adolescent resilience scale diffusion-tensor imaging (ars-DTI) tensor image in panel (**c**). Overall image quality was rated "good" for readout-segmented echo planar diffusion-tensor imaging (rs-DTI) and "moderate" for ss-DTI by both readers. Ghosting artifacts in opposite were found to be "low"[2] in ss-DTI and "moderate"[3] in rs-DTI by both readers.

Mean FA measured by the two readers, at all brachial plexus levels, for both DTI sequences is also reported. CNR, SNR, and FA values were tested for normal distribution using the Shapiro-Wilk test. The paired *t*-tests were performed to evaluate for statistically significant differences regarding CNR, SNR, and FA measured with ss-DTI versus rs-DTI. Intraclass correlation coefficients (ICCs) were calculated for evaluating the inter-reader agreement of SNR and CNR analyses and FA measurements. ICC values were interpreted as follows: the inter-reader agreement was assumed to be excellent for values greater than 0.75, fair to good for values between 0.40 and 0.75 and poor for values below 0.40.[23]

Qualitative image analysis

Cohen's kappa was applied to evaluate inter-reader agreement in the qualitative evaluation of geometrical distortions, ghosting/motion artifacts, resolution, and overall image quality. Cohen's kappa values were interpreted according to Landis and Koch as follows:[24] Kappa values above 0.8 corresponded to an excellent agreement, values between 0.6 and 0.8 to substantial levels of agreement, values from 0.4 to 0.6 moderate agreement, and values below 0.4 poor to fair agreement.

P values < 0.05 were considered to indicate a significant difference and Bonferroni correction was applied in case of multiple comparisons.

Results

All morphological and diffusion-weighted images (DWIs) were acquired in all subjects without exceeding the specific absorption rate (SAR) limits. Mean values of SNR and CNR measurements, obtained from the two DTI sequences are reported in Table 2. Mean FA values obtained from C5 to T_1 are reported in Table 3.

SNR analysis

Mean SNR values measured with rs-DTI and ss-DTI sequence were similar for both readers (Table 2, $P = 0.558$ for reader 1 and $P = 0.457$ for reader 2). The Inter-reader agreement was "fair to good" for ss-DTI with ICC 0.452 ($P = 0.0192$) and "excellent" for rs-DTI with ICC 0.898 ($P < 0.001$).

Table 2 Quantitative CNR and SNR analysis

	ss-DTI		rs-DTI		ss-DTI vs. rs-DTI
	Mean	SD	Mean	SD	*P*-value
Reader 1					
SNR	6.08	2.35	6.57	2	0.558
CNR	0.5	0.11	0.52	0.09	0.624
Reader 2					
SNR	6.1	2.53	6.49	1.97	0.475
CNR	0.5	0.1	0.54	0.1	0.709

For both sequences and readers, CNR and SNR are given as mean ± SD. Paired *t*-tests were performed to assess potential between group differences. CNR, contrasttonoise ratio; rs-DTI, readout-segmented echo planar diffusion-tensor imaging; SD, standard deviation; SNR, signal-to-noise ratio; ss-DTI, single-shot echo planar diffusion-tensor imaging.

CNR analysis

Mean CNR values obtained with rs-DTI and ss-DTI sequences were not significantly different for both readers (Table 2, $P = 0.624$ for reader 1 and $P = 0.709$ for reader 2). Inter-reader agreement was "excellent" for both ss-DTI with ICC 0.974 ($P < 0.001$) and rs-DTI with ICC 0.995 ($P < 0.001$).

Fractional anisotropy

ss-DTI FA values ranged from (mean ± SD) 0.337 ± 0.022 of left T_1 to 0.396 ± 0.017 of left C5 for reader 1 and from 0.353 ± 0.030 of left T_1 to 0.383 ± 0.030 of left C7 for reader 2. Rs-DTI FA values ranged from 0.347 ± 0.022 of left C8 to 0.389 ± 0.029 of right T_1 for reader 1 and from 0.352 ± 0.024 of left T_1 to 0.384 ± 0.034 of left C5 for reader 2 (Table 3). FA-values obtained from ss-DTI and rs-DTI at all levels were similar for both readers (reader 1: $P = 0.035$–0.958; reader 2: $P = 0.169$–0.944).

Table 3 Quantitative diffusion analysis

	ss-DTI		rs-DTI		ss-DTI vs. rs-DTI
	Mean	SD	Mean	SD	*P*-value
Reader 1					
C5 Right	0.379	0.027	0.372	0.026	0.573
C5 Left	0.396	0.017	0.376	0.022	0.035
C6 Right	0.372	0.018	0.382	0.032	0.379
C6 Left	0.365	0.027	0.364	0.038	0.958
C7 Right	0.371	0.018	0.384	0.031	0.274
C7 Left	0.38	0.028	0.361	0.035	0.195
C8 Right	0.385	0.024	0.38	0.035	0.7
C8 Left	0.355	0.024	0.347	0.034	0.551
T_1 Right	0.38	0.028	0.389	0.029	0.49
T_1 Left	0.337	0.022	0.352	0.029	0.187
Total	0.372	0.023	0.371	0.031	
Reader 2					
C5 Right	0.377	0.014	0.376	0.028	0.944
C5 Left	0.368	0.039	0.384	0.034	0.35
C6 Right	0.38	0.016	0.366	0.026	0.169
C6 Left	0.364	0.031	0.354	0.037	0.528
C7 Right	0.373	0.026	0.358	0.044	0.385
C7 Left	0.383	0.03	0.359	0.052	0.214
C8 Right	0.374	0.034	0.378	0.015	0.709
C8 Left	0.367	0.03	0.363	0.033	0.754
T_1 Right	0.366	0.024	0.38	0.027	0.229
T_1 Left	0.353	0.03	0.352	0.024	0.974
Total	0.370	0.027	0.367	0.032	

For each sequence and reader, FA values are shown as mean ± SD for each level of the brachial plexus from C5 to TH1 for both sides. Paired sample *t*-tests were performed to assess potential between group differences. Corresponding *P*-values are given. rs-DTI, readout-segmented echo planar diffusion-tensor imaging; SD, standard deviation; ss-DTI, single-shot echo planar diffusion-tensor imaging.

Inter-reader agreement of FA measurements ranged from "poor" to "excellent" for conventional ss-DTI with ICC 0.064 ($P = 0.461$) to ICC 0.905 ($P = 0.013$), at level of C8 left and T_1 right, respectively. Similarly, rs-DTI FA measurements ranged from "poor" to "moderate" for conventional ss-DTI with ICC 0.065 ($P = 0.461$) to ICC 0.770 ($P = 0.02$) at level of C6 right and C5 right, respectively.

For all root-levels of both sides, the inter-reader agreement measured moderate agreement for ss-DTI, as well as rs-DTI with ICC = 0.69 (95% CI = 0.33–0.93) and ICC = 0.72 (95% CI = 0.063–0.93), respectively.

Qualitative analysis

Distortion artifacts scores were rated significantly higher in ss-DTI than in rs-DTI for both readers ($P = 0.001$ for reader 1 and $P = 0.002$ for reader 2) (Table 4 and Fig. 2). In the evaluation of ghosting/motion artifacts and resolution, no significant differences were found between both sequences for both readers ($P > 0.121$ for reader 1 and $P > 0.264$ for reader 2). A "substantial" to "excellent" agreement was observed in the evaluation of the distortion artifact (ss-DTI, kappa, 0.851; rs-DTI kappa 0.782), a "moderate" inter-observer agreement was observed for ghosting/motion artifacts (ss-DTI, kappa, 0.50; rs-DTI, kappa, 0.40) and a "moderate" inter-observer agreement was observed for the resolution (ss-DTI, kappa, 0.50; rs-DTI, kappa, 0.60). Overall image quality was rated significantly higher in ss-DTI than in rs-DTI for both readers ($P = 0.001$ for reader 1 and $P = 0.002$ for reader 2, Table 4 and Fig. 3) and a "substantial" to "excellent" agreement (ss-DTI, kappa, 0.69; rs-DTI, kappa, 0.825) was observed.

Discussion

DWI and in particular DTI has the potential to become an important component of MRI of the brachial plexus, enhancing detection and localization of various plexopathies.[1,11–13] To date, DTI is not routinely applied for the evaluation of the brachial plexus in clinical practice. Besides a lack of reliable data, which would support the interpretation of obtained DTI

Table 4 Qualitative analysis

	ss-DTI		rs-DTI		ss-DTI vs. rs-DTI
	Mean	SD	Mean	SD	*P*-value
Reader 1					
Distortion artifacts	3.4	0.663	2.3	0.458	*0.001*
Ghosting/ Motion artifacts	2.5	0.5	3.0	0.572	0.121
Resolution	2.7	0.458	2.4	0.490	0.196
Overall image quality	3.2	0.6	2.3	0.458	*0.002*
Reader 2					
Distortion artifacts	3.5	0.671	2.5	0.5	*0.002*
Ghosting/ Motion artifacts	2.5	0.500	2.8	0.6	0.264
Resolution	2.8	0.748	2.5	0.5	0.331
Overall image quality	3.3	0.458	2.2	0.4	*0.001*

Grading of distortion artifacts, ghosting/motion artifacts, resolution and overall image quality is provided for each sequence and reader as mean ± SD on a 5-point Likert scale (artifacts: 1, none; 2, low; 3, moderate; 4, high; 5, very high; overall image quality: 1, excellent; 2, good; 3, moderate; 4, poor; 5, non-diagnostic). Paired *t*-tests were performed to assess potential group differences. Corresponding *P*-values are given. Italics indicate statistical significance.

metrics in diagnostic and their application on clinical decision making, technical aspects as robustness and image quality of DTI sequences inter alia distortion artifacts, motion artifacts, and limited SNR are still considerable restraints. In order to contribute to the DTI improvement for future diagnostic application, we evaluated an advanced DTI technique in which an innovative excitation and sampling method were adopted. The same technique showed promising results when high-resolution DTI had been applied in the evaluation of the median nerve,[25] the brain,[26] the pelvis[18] and the breast,[27] in comparison to the current reference standard of DTI sequences. New rs-DTI was assessed quantitatively regarding SNR, CNR, and FA and qualitatively regarding geometrical distortions, ghosting/motion artifacts, resolution and overall image quality in 10 healthy volunteers. Our results show that both techniques, rs-DTI and ss-DTI, robustly imaged the structures of the supraclavicular brachial plexus in comparable times of acquisition, suited for clinical routine.

For both DTI sequences, SNR was similar, but slightly better in rs-DTI. SNR is dependent on several factors-among them voxel size, number of directions, number of averaged excitations[28] and *b*-values.[29] Given comparable prerequisites regarding these parameters, this statistically non-significant trend toward a better SNR for rs-DTI has to be proofed in further studies.

CNR values too did not differ significantly between sequences, although the signal of nerve structure and the contrast between the trunks, and surrounding tissue was notably higher for rs-DTI compared to ss-DTI. This contrast is of particular importance for sensitivity of measurements, when focal or asymmetrical, potentially pathological signal alterations in diffusion metrics along nerve structures in brachial plexus are to be detected.

Quantitative, ROI-based FA measurements itself in the post-ganglionic trunks did not significantly differ between the evaluated DTI techniques except the level C5 on the left side for reader 1. But absolute FA values at this level were within the range of FA values at other levels and standard deviations were comparably low. Regarding the inter-reader agreement for all root levels on both sides the only marginal difference was measured between the evaluated DTI techniques.

In comparison, the FA-values measured in healthy volunteers of this study (mean ± SD; 0.337 ± 0.022 to 0.396 ± 0.017) are in accordance with recent literature, where FA means for healthy controls for cervical nerve roots ranged from 0.265 to 0.367.[11,14] Diffusion metrics including FA have been proven to have a high test-retest reliability and reproducibility in the brachial plexus underuse of identical hard- and software.[30] However, significant differences in diffusion metrics can be expected in the peripheral nervous system between vendors of hard- and software.[31,32]

Overall image quality was significantly better and severity of distortion artifacts was significantly lower for rs-DTI compared to ss-DTI. Results also suggest a trend toward a better resolution for rs-DTI. Previous studies have described readout-segmented diffusion as a robust technique for quantitative imaging especially in areas physiologically prone to distortion- and susceptibility artifacts.[18,21] A trend toward more ghosting artifacts on rs-DTI compared to ss-DTI can be partially explained by the segmented filling of *k*-space data in temporally separated steps.[19]

Limitations

Several limitations of the current study have to be acknowledged. (i) Sample size. Only 10 healthy volunteers were included, but in general sample size was similar to other studies addressing the assessment and feasibility of new diffusion sequences.[22,25,33] In addition, all data were consistent with comparably low standard deviations. Thus, we do not assume a larger sample size would have changed the results of this study. Solely asymptomatic healthy volunteers were assessed since it was considered mandatory due to ethical reasons and with respect to the time-consuming study protocol to first gather robust data concerning the characteristics of the new rs-DTI sequence applied in the brachial plexus before investigating a patient population. (ii) Study population. Only one subject reached 40 years of age, while the study group was 31 years in the mean. Age does affect quantitative metrics, since diffusion properties are known to change with age. Therefore, further investigation, in older and possibly in symptomatic individuals has to be conducted to assess the impact on their significance of DTI parameters.[34] Although adequate inter-rater ICC is given, another limitation of this study is a possibly reduced reproducibility of ROI determination, defining ROIs in relatively low-resolution TRACE image.

Conclusion

Our study supports the hypothesis that DTI with innovative readout-segmented diffusion sequences with navigator-echo correction yield significantly better overall image quality and lead to fewer distortion artifacts compared to the current reference of diffusion imaging in the brachial plexus. Results permit the application of rs-DTI for future functional MRN of the brachial plexus in a reasonable scan time for routine clinical practice.

Further studies in patients with a large variety of different pathologies are desirable to evaluate the potential clinical impact of DTI in the brachial plexus.

Ethical Approval

All procedures performed in the studies involving human participants were in accordance with the ethical standards of the institutional and national research committee and with

the 1964 Helsinki Declaration and its later amendments or comparable ethical standards. Informed consent was obtained from all individual participants included in the study.

Conflicts of Interest

The authors declare that they have no conflicts of interest. No funding was received for this study.

References

1. Vargas MI, Gariani J, Delattre BA, Dietemann JL, Lovblad K, Becker M. Three-dimensional MR imaging of the brachial plexus. Semin Musculoskelet Radiol 2015; 19:137–148.
2. Chhabra A, Thawait GK, Soldatos T, et al. High-resolution 3T MR neurography of the brachial plexus and its branches, with emphasis on 3D imaging. AJNR Am J Neuroradiol 2013; 34:486–497.
3. Upadhyaya V, Upadhyaya DN, Kumar A, Gujral RB. MR neurography in traumatic brachial plexopathy. Eur J Radiol 2015; 84:927–932.
4. Tagliafico A, Succio G, Serafini G, Martinoli C. Diagnostic accuracy of MRI in adults with suspect brachial plexus lesions: a multicentre retrospective study with surgical findings and clinical follow-up as reference standard. Eur J Radiol 2012; 81:2666–2672.
5. Du R, Auguste KI, Chin CT, Engstrom JW, Weinstein PR. Magnetic resonance neurography for the evaluation of peripheral nerve, brachial plexus, and nerve root disorders. J Neurosurg 2010; 112:362–371.
6. Chhabra A, Belzberg AJ, Rosson GD, et al. Impact of high resolution 3 tesla MR neurography (MRN) on diagnostic thinking and therapeutic patient management. Eur Radiol 2016; 26:1235–1244.
7. Gasparotti R, Lodoli G, Meoded A, Carletti F, Garozzo D, Ferraresi S. Feasibility of diffusion tensor tractography of brachial plexus injuries at 1.5 T. Invest Radiol 2013; 48:104–112.
8. Chhabra A, Gustav A, ed. Magnetic resonance neurography. 1st ed. New Delhi: Jaypee Brothers Medical Pub; 2012.
9. Eguchi Y, Ohtori S, Orita S, et al. Quantitative evaluation and visualization of lumbar foraminal nerve root entrapment by using diffusion tensor imaging: preliminary results. AJNR Am J Neuroradiol 2011; 32:1824–1829.
10. Dallaudière B, Lincot J, Hess A, et al. Clinical relevance of diffusion tensor imaging parameters in lumbar disco-radicular conflict. Diagn Interv Imaging 2014; 95:63–68.
11. Chen YY, Lin XF, Zhang F, et al. Diffusion tensor imaging of symptomatic nerve roots in patients with cervical disc herniation. Acad Radiol 2014; 21:338–344.
12. Yuh EL, Jain Palrecha S, Lagemann GM, et al. Diffusivity measurements differentiate benign from malignant lesions in patients with peripheral neuropathy or plexopathy. AJNR Am J Neuroradiol 2015; 36:202–209.
13. Andreou A, Sohaib A, Collins DJ, et al. Diffusion-weighted MR neurography for the assessment of brachial plexopathy in oncological practice. Cancer Imaging 2015; 15:6.
14. Vargas MI, Viallon M, Nguyen D, Delavelle J, Becker M. Diffusion tensor imaging (DTI) and tractography of the brachial plexus: feasibility and initial experience in neoplastic conditions. Neuroradiology 2010; 52: 237–245.
15. Porter DA, Heidemann RM. High resolution diffusion-weighted imaging using readout-segmented echo-planar imaging, parallel imaging and a two-dimensional navigator-based reacquisition. Magn Reson Med 2009; 62:468–475.
16. Holdsworth SJ, Skare S, Newbould RD, Bammer R. Robust GRAPPA-accelerated diffusion-weighted readout-segmented (RS)-EPI. Magn Reson Med 2009; 62:1629–1640.
17. Azuma T, Kodama T, Yano T, Enzaki M, Nakamura M, Murata K. Optimal imaging parameters for readout-segmented EPI of the temporal bone. Magn Reson Med Sci 2015; 14:145–152.
18. Thian YL, Xie W, Porter DA, Weileng Ang B. Readout-segmented echo-planar imaging for diffusion-weighted imaging in the pelvis at 3T-A feasibility study. Acad Radiol 2014; 21:531–537.
19. Barth BK, Cornelius A, Nanz D, Eberli D, Donati OF. Diffusion-weighted imaging of the prostate: image quality and geometric distortion of readout-segmented versus selective-excitation accelerated acquisitions. Invest Radiol 2015; 50:785–791.
20. Morelli J, Porter D, Ai F, et al. Clinical evaluation of single-shot and readout-segmented diffusion-weighted imaging in stroke patients at 3 T. Acta Radiol 2013; 54: 299–306.
21. Drubach LA, Zurakowski D, Palmer EL, Tracy DA, Lee EY. Utility of salivagram in pulmonary aspiration in pediatric patients: comparison of salivagram and chest radiography. AJR Am J Roentgenol 2013; 200:437–441.
22. Manoliu A, Ho M, Nanz D, et al. Diffusion tensor imaging of lumbar nerve roots: comparison between fast readout-segmented and selective-excitation acquisitions. Invest Radiol 2016; 51:499–504.
23. Borich MR, Wadden KP, Boyd LA. Establishing the reproducibility of two approaches to quantify white matter tract integrity in stroke. Neuroimage 2012; 59: 2393–2400.
24. Landis JR, Koch GG. The measurement of observer agreement for categorical data. Biometrics 1977; 33:159–174.
25. Filli L, Piccirelli M, Kenkel D, et al. Accelerated magnetic resonance diffusion tensor imaging of the median nerve using simultaneous multi-slice echo planar imaging with blipped CAIPIRINHA. Eur Radiol 2016; 26:1921–1928.
26. Holdsworth SJ, Yeom K, Skare S, Gentles AJ, Barnes PD, Bammer R. Clinical application of readout-segmented-echo-planar imaging for diffusion-weighted imaging in pediatric brain. AJNR Am J Neuroradiol 2011; 32:1274–1279.
27. Filli L, Ghafoor S, Kenkel D, et al. Simultaneous multi-slice readout-segmented echo planar imaging for accelerated diffusion-weighted imaging of the breast. Eur J Radiol 2016; 85:274–278.
28. Santarelli X, Garbin G, Ukmar M, Longo R. Dependence of the fractional anisotropy in cervical spine from the number of diffusion gradients, repeated acquisition and voxel size. Magn Reson Imaging 2010; 28:70–76.

29. Guggenberger R, Eppenberger, Markovic D, et al. MR neurography of the median nerve at 3.0T: optimization of diffusion tensor imaging and fiber tractography. Eur J Radiol 2012; 81:e775–e782.
30. Ho MJ, Manoliu A, Kuhn FP, et al. Evaluation of reproducibility of diffusion tensor imaging in the brachial plexus at 3.0 T. Invest Radiol 2017; 52:482–487.
31. Guggenberger R, Nanz D, Bussmann L, et al. Diffusion tensor imaging of the median nerve at 3.0 T using different MR scanners: agreement of FA and ADC measurements. Eur J Radiol 2013; 82:e590–e596.
32. Guggenberger R, Nanz D, Puippe G, et al. Diffusion tensor imaging of the median nerve: intra-, inter-reader agreement, and agreement between two software packages. Skeletal Radiol 2012; 41:971–980.
33. Zhou Y, Narayana PA, Kumaravel M, Athar P, Patel VS, Sheikh KA. High resolution diffusion tensor imaging of human nerves in forearm. J Magn Reson Imaging 2014; 39:1374–1383.
34. Guggenberger R, Markovic D, Eppenberger P, et al. Assessment of median nerve with MR neurography by using diffusion-tensor imaging: normative and pathologic diffusion values. Radiology 2012; 265:194–203.